ACS Photonics

pubs.acs.org/journal/apchd5

Article

Wavelength-Switchable Positive and Negative Photoconductivity in a Ge/Si Heterojunction Nanowire

Huayou Liu, Jing Zhang, Jie-yin Zhang, Jiayuan Zhao, Constantinos Valagiannopoulos, Daniele Tosi, Jian-jun Zhang, Zhijuan Su,* and Yaping Dan*

Cite This: https://doi.org/10.1021/acsphotonics.5c02680

Read Online

ACCESS | Metrics & More | Article Recommendations | Supporting Information

ABSTRACT: The development of silicon-compatible, high-performance infrared photodetectors is crucial for advancing thermal imaging, security, and communication systems. While germanium is a promising near-infrared material, its behavior in nanostructured forms with silicon heterojunctions reveals complex photophysics. This work demonstrates a germanium nanowire photodetector grown on a silicon-on-insulator (SOI) platform that exhibits a striking, tunable coexistence of both positive photoconductivity (PPC) and negative photoconductivity (NPC). We show that the dominant photoresponse can be switched by the wavelength of incident light: NPC dominates at visible wavelengths (e.g., 532 nm), while PPC prevails in the near-infrared (e.g., 1310 nm). Through systematic experiments and FDTD and TCAD simulations, we elucidate that this phenomenon arises from the interplay of light absorption in the different layers of the heterostructure. At short wavelengths, strong absorption in the underlying Si layer forward-biases the heterojunction, injecting carriers that quench the Ge channel conductance (NPC). At long wavelengths, absorption is confined to the Ge layer, resulting in conventional PPC. Negative photoconductivity was consistently observed over the temperature range from 78 to 298 K. Notably, the maximum responsivity of the nanowire increased from −56.7 A/W at room temperature to −1421.5 A/W at 78 K. This is attributed to the suppression of surface recombination velocity, increasing the minority carrier lifetime by 2 orders of magnitude. The −3 dB bandwidth is 2.9 kHz under 532 nm light and 3.9 kHz under 1310 nm light. The minimum noise equivalent power is determined to be 5.3×10^{-14} W/Hz$^{0.5}$, corresponding to a specific detectivity of 4.0×10^{9} Jones at room temperature. Furthermore, we demonstrate that the crossover wavelength is intensity-dependent and that the photocurrent follows an established logarithmic model for nanowire photoconductors. This work provides a controllable model system for studying NPC and presents a novel device architecture with tunable, multifunctional photoresponse for advanced optoelectronic applications.

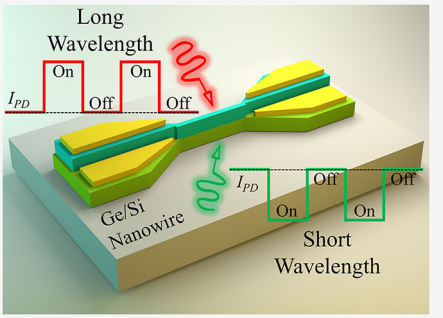

KEYWORDS: *Negative Photoconductivity, Ge/Si Heterojunction, Nanowire, Photodetector*

INTRODUCTION

The relentless demand for high-performance, silicon-compatible infrared photodetection, driven by applications in thermal imaging,[1] environmental monitoring,[2] and secure communications,[3] has intensified the search for advanced materials and device architectures.[4,5] While group III−V semiconductors like InGaAs offer excellent infrared performance, their integration with mainstream silicon CMOS technology remains challenging and costly.[6,7] Germanium (Ge) has emerged as a compelling alternative, offering a narrow bandgap suitable for near-infrared detection (up to 1600 nm), high carrier mobilities, and full compatibility with silicon fabrication platforms.[8−10]

However, as device dimensions shrink to the nanoscale, novel and often counterintuitive photophysical phenomena emerge. Among these, Negative Photoconductivity (NPC)—a decrease in electrical conductivity upon light illumination—presents a significant scientific puzzle and a potential opportunity for new device functionalities.[11−13] NPC stands in stark contrast to the ubiquitous Positive Photoconductivity (PPC) observed in conventional semiconductors. Over the past decade, NPC has been reported across a diverse range of low-dimensional materials, including indium arsenide (InAs) nanowires,[14] transition metal dichalcogenides (TMDs),[15] carbon nanotubes (CNTs),[16] and germanium sulfide (GeS).[17]

The physical origins of NPC are complex and often system-dependent, leading to several proposed mechanisms. As summarized by Tailor et al.,[13] these hypotheses include: (i) deep-level excitation, where photoexcited carriers are trapped by defect states, effectively reducing the number of free carriers; (ii) hot electron trapping, where highly energetic

Received: November 6, 2025
Revised: January 7, 2026
Accepted: January 7, 2026

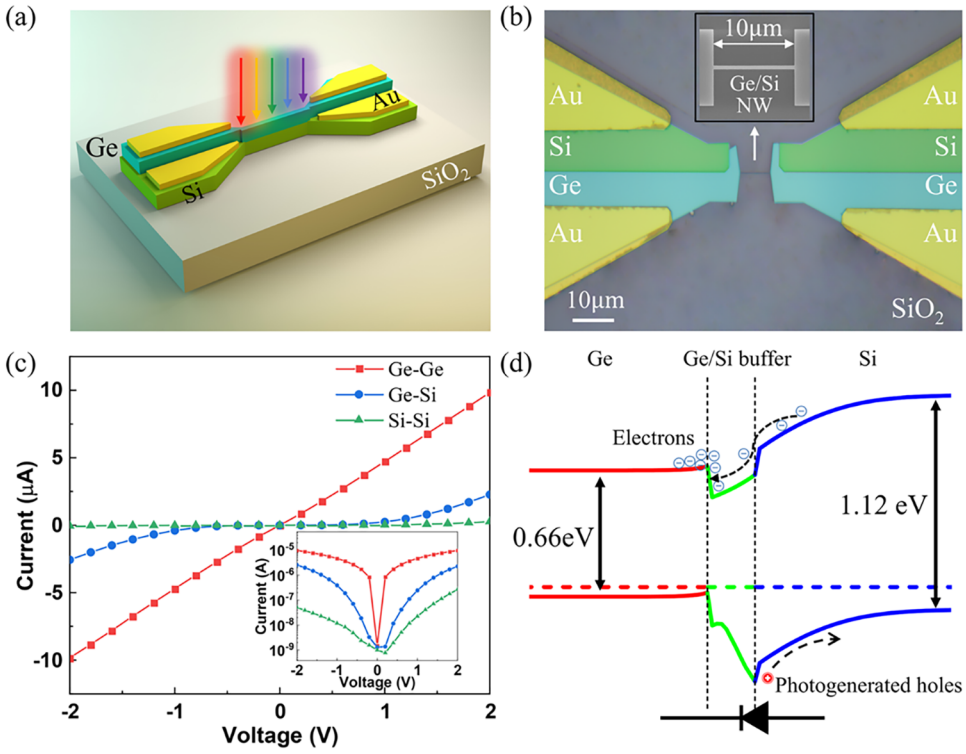

Figure 1. (a) and (b) Schematic and microscope image of Ge on SOI nanowire photodetector, respectively. Inset: SEM image of the nanowire. This nanowire is 10 μm long and 250 nm wide. (c) Dark $I-V$ curves of Ge/Si nanowires using different combinations of electrodes. Inset: logarithmic scale of current of these curves. (d) Energy band diagram of Ge/Si nanowire using Silvaco TCAD simulation.

carriers scatter into immobilized states; (iii) photothermal effects, where light-induced heating increases phonon scattering and reduces mobility; (iv) surface adsorption/desorption of molecules like water vapor, altering surface band bending; (v) trion formation, where the binding of an additional charge carrier reduces overall mobility; and (vi) DX-like centers, specific defect complexes that undergo a large lattice relaxation upon carrier capture. This diversity of mechanisms underscores a critical challenge in the field: the lack of a universal, controllable model system to conclusively isolate and study a single NPC mechanism. Many reported instances of NPC are either irreversible, unstable, or difficult to reproduce, limiting their potential for practical applications.

In this work, we address this fundamental challenge by designing and fabricating a well-defined Ge/Si heterojunction nanowire photodetector on a Silicon-on-Insulator (SOI) platform. This architecture not only provides a stable and CMOS-compatible infrared photodetector but also serves as a unique testbed for investigating NPC. We report the controlled and reversible coexistence of both PPC and NPC within a single device, where the dominant photoresponse can be deterministically switched by the wavelength of incident light. Through a combination of experimental photocurrent measurements across different electrode configurations, different temperatures, different frequencies, together with Ansys FDTD and Silvaco TCAD simulations, we demonstrate that the observed NPC is not driven by the more common mechanisms of defect trapping or photothermal heating. Instead, we unveil a photogating effect mediated by the heterojunction interface: under short-wavelength illumination, strong absorption in the underlying silicon layer forward-biases the heterojunction, injecting carriers that quench the conductance of the Ge channel. This mechanism provides a clear, electrically tunable pathway for NPC.

RESULTS AND DISCUSSIONS

The schematic of a Ge/Si nanowire photodetector is shown in Figure 1(a). The fabrication process details, testing, and simulation methods can be found in the Sections I and II of Supporting Information (SI). An optical microscope image of a representative nanowire is shown in Figure 1(b). We also captured scanning electron microscopy and energy dispersive X-ray spectroscopy images to characterize the morphology and elemental distribution of the device (see SI Section III). The red line (Ge−Ge) in Figure 1(c) corresponds to the current measured between the two electrodes contacting the top Ge layer. Additional $I-V$ curves and dependence of the dark current on the nanowire channel width are provided in the Section IV of SI. The linear $I-V$ characteristics indicate that the metal−Ge contacts are ohmic and that the Ge channel is electrically continuous. The green curve (Si−Si) represents the current measured between the pair of electrodes contacting the underlying Si layer. The current is mostly linear but relatively small because the Si channel is nearly depleted due to its relatively low doping concentration and small thickness (220 nm). The energy band diagram of the Ge/Si heterojunction nanowire is simulated using Silvaco TCAD software as shown in Figure 1(d). The complex refractive index of these layer stacks was determined by a spectroscopic ellipsometer (see SI Section V). The energy bandgap of Ge and Si calculated from the Tauc plot is 0.69 and 1.09 eV, respectively. The bandgap energies of the buffer layer derived from the extinction coefficient yielded multiple characteristic values of 0.69, 0.82, and 1.03 eV. It is worth noting that, these values represent spatially averaged quantities rather than absolute bandgap

https://doi.org/10.1021/acsphotonics.5c02680
ACS Photonics XXXX, XXX, XXX−XXX

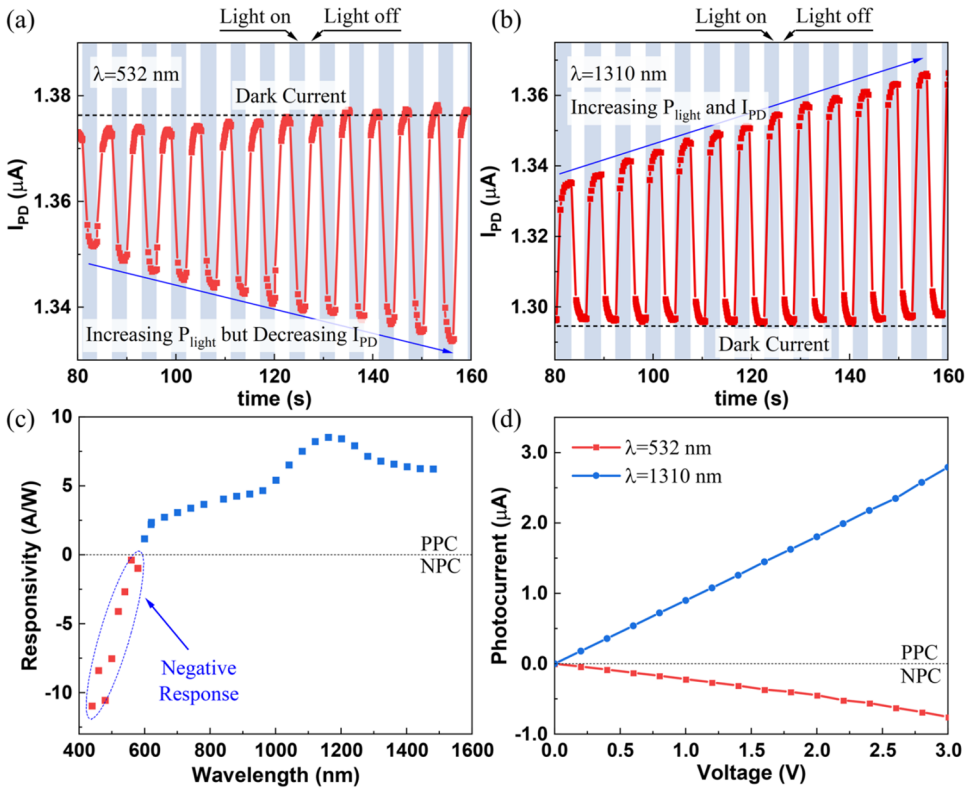

Figure 2. Transient photoresponses of the Ge/Si nanowire at different wavelengths: (a) 532 nm and (b) 1310 nm. (c) Spectral response of the Ge/Si nanowire. The nanowire is applied with a fixed bias voltage of 0.1 V in (a–c). (d) Photocurrent as a function of bias voltage. The nanowire used here has a channel width of 450 nm and a length of 10 μm.

energies at specific spatial locations. These values fall between those of Ge and Si, consistent with the physical characteristics of SiGe alloys. It should be pointed out that in the Silvaco TCAD simulation, we cannot set a material that has three bandgap energies. Therefore, during the simulation, empirical equations obtained by fitting the experimental bandgap energy of $Si_{1-x}Ge_x$ alloy material were adopted. Anyway, what we really need is its properties as an n-type semiconductor. Hall measurement results reveal that the Ge and Si layers are p-type, and the $Si_{1-x}Ge_x$ buffer layer is n-type (see SI Section VI). The work-function difference in this trilayer structure induces depletion regions in both the Ge and Si layers, leading to full depletion of the thin n-type $Si_{1-x}Ge_x$ buffer. The depleted n-type buffer layer forms a weak p–n–p structure, which is insufficient to block carrier transport across the heterostructure. For this reason, the current flowing across the Ge/Si heterogeneous junction is highly nonlinear (blue line in Figure 1(c)).

Interestingly, when using the top germanium as the electrical contact, the nanowire exhibits negative photoresponses under short-wavelength illumination but positive photoresponses under long-wavelength illumination, as shown in Figure 2(a,b), respectively. For the negative photoresponse in Figure 2(a), the current at a fixed bias decreased upon illumination and returned to its dark current once the light was turned off. In contrast, for positive photoresponse in Figure 2(b), the current increased under illumination and returned to its original dark current when the light was cut off. More positive and negative photoconductivity data for nanowire devices of different widths can be found in SI Section VII. To further validate this observation, we employed a monochromator to measure the spectral response of the nanowire, as shown in Figure 2(c). It is worth noting that, during the spectral response measurements, relatively high optical intensities were required in order to obtain sufficiently large photocurrents, resulting in responsivities of only a few A/W. In fact, the Ge/Si nanowire photodetectors fabricated in this work are capable of exhibiting maximum responsivities exceeding 10^5 A/W (see SI Section VIII). The corresponding external quantum efficiency (EQE) exceeds 2×10^5 in this case. Nevertheless, achieving extremely high photoresponsivity is beyond the scope of this work and is therefore not discussed in detail here. The photoresponse shifts from negative to positive as the wavelength increases across ~600 nm. This crossing wavelength actually depends on light intensity, which will be discussed later. Indeed, the photocurrent is negatively and positively dependent on the bias voltage at λ = 532 and 1310 nm, respectively, as shown in Figure 2(d). According to our previous finding, the photocurrent will eventually saturate due to the metal–semiconductor boundary confinement as the applied voltage increases.[18] This saturation phenomenon occurs when the drift length is comparable to the nanowire length. We analyze this saturation condition as follows. For our Ge/Si nanowires at a doping concentration of 7.41×10^{17} cm^{-3}, the electron and hole mobilities in Ge are around 2000 cm^2V/s.[19,20] Due to the strong surface recombination in nanowires, the effective diffusion length L_D of electrons and holes are comparable to the nanowire width (~300 nm) with $L_D = \sqrt{D\tau}$ in which D is the diffusivity and τ is the effective minority recombination lifetime. Given $D = \mu\frac{k_B T}{q}$ with k_B being the Boltzmann constant, T the absolute temperature,

https://doi.org/10.1021/acsphotonics.5c02680
ACS Photonics XXXX, XXX, XXX–XXX

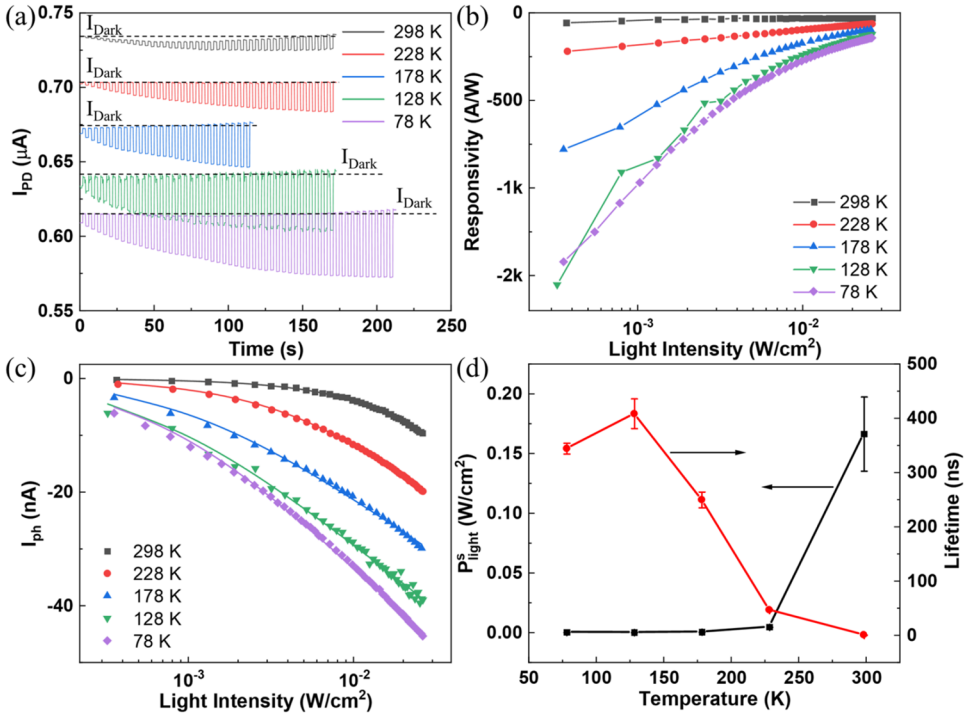

Figure 3. (a) The temperature dependence of the negative photoconductivity of Ge/Si nanowires under 532 nm light. The black dashes are the view guide of the dark current. (b) The responsivity and (c) the photocurrent as a function of light intensity at different temperatures. The solid lines in (c) are the fitting results using eq 1. (d) The extracted critical light intensity P^s_{light} and effective minority carrier lifetime at different temperatures. The nanowire used here has a channel width of 250 nm and a length of 10 μm at a fixed bias voltage of 0.1 V.

and q the unit charge, the effective minority recombination lifetime is estimated as 17 ps. The photocurrent saturation occurs when the drift length $L_{dr} = \mu E\tau$ is approximately equal to the nanowire length L. To observe this photocurrent saturation phenomenon, the voltage must be increased to 0.29 V, 29.4 and 264.7 V when the nanowire lengths are 1 μm, 10 and 30 μm, respectively. This explains why the photocurrent is linearly dependent on the voltage in Figure 2(d) for our 10 μm long nanowire in a bias range of 0−3 V. When the nanowire length is reduced to 1 μm, the photocurrent saturation phenomenon can be readily observed (see SI Section IX).

Another widely reported mechanism for negative photoconductive responses is the photothermal effect.[21] Optical illumination induces device heating, thereby reducing carrier mobility and the overall electrical conductivity. However, this mechanism is unlikely to account for the negative photoconductivity observed in the Ge/Si nanowires. First, to minimize thermal effects, a square-wave modulation was applied to periodically switch the light source on and off during the measurements, rather than a continuous illumination on the device. Second, the optical intensity of the 1310 nm light source employed in the measurements was, in fact, higher than that of the 532 nm light source. Logically, if photothermal heating were the dominant mechanism, a stronger negative photoresponse would be expected under 1310 nm illumination rather than under 532 nm illumination. This expectation is in direct contradiction with the experimental observations, where negative photoconductivity was observed only under 532 nm illumination. In addition, the device under test was not only protected as much as possible from external light sources and electromagnetic waves but also directly fixed on a sample stage with high thermal conductivity, which greatly improves the heat dissipation efficiency of the device. More direct evidence is provided by the temperature-dependent photoresponse measurements, as shown in Figure 3. Negative photoconductivity is consistently observed over the temperature range from 78 to 298 K. Notably, as the temperature decreases, the on/off ratio, responsivity, and optical gain of the device all increase, as illustrated in Figure 3(b). At an incident optical intensity of 0.36 mW/cm^2, the maximum responsivity of the nanowire increases from −56.7 A/W at room temperature to −1421.5 A/W at 78 K. Accordingly, the EQE increases from 6400% to 160,500%. This is consistent with the trend of photoconductive devices reported in other literatures.[22−24] The enhancement in responsivity with decreasing temperature is attributed to the increase in the effective minority carrier lifetime. The photoresponses of the Ge and Si channels will also follow the photoresponse theory we established previously for nanowire photoconductors, as shown in eq 1[18,25,26]

$$I_{ph} = I_{th} \ln\left(\frac{P_{light}}{P^s_{light}} + 1\right) \tag{1}$$

where I_{th} is the threshold photocurrent. $P^s_{light} = \frac{\hbar\omega n_i W}{2\alpha\tau_0}$ is the critical light intensity, with $\hbar\omega$ being the photon energy, n_i being the intrinsic carrier concentration, W being the width of the nanowire, α being the light absorption ratio, τ_0 being the effective minority carrier lifetime. By fitting the experimental photocurrent−light intensity curves at different temperatures, as shown in Figure 3(c), the critical light intensity and minority carrier lifetime are extracted in Figure 3(d). The fitting results indicate that, as the temperature decreases from 298 to 78 K, the minority carrier lifetime increases from 1.4 to

https://doi.org/10.1021/acsphotonics.5c02680
ACS Photonics XXXX, XXX, XXX−XXX

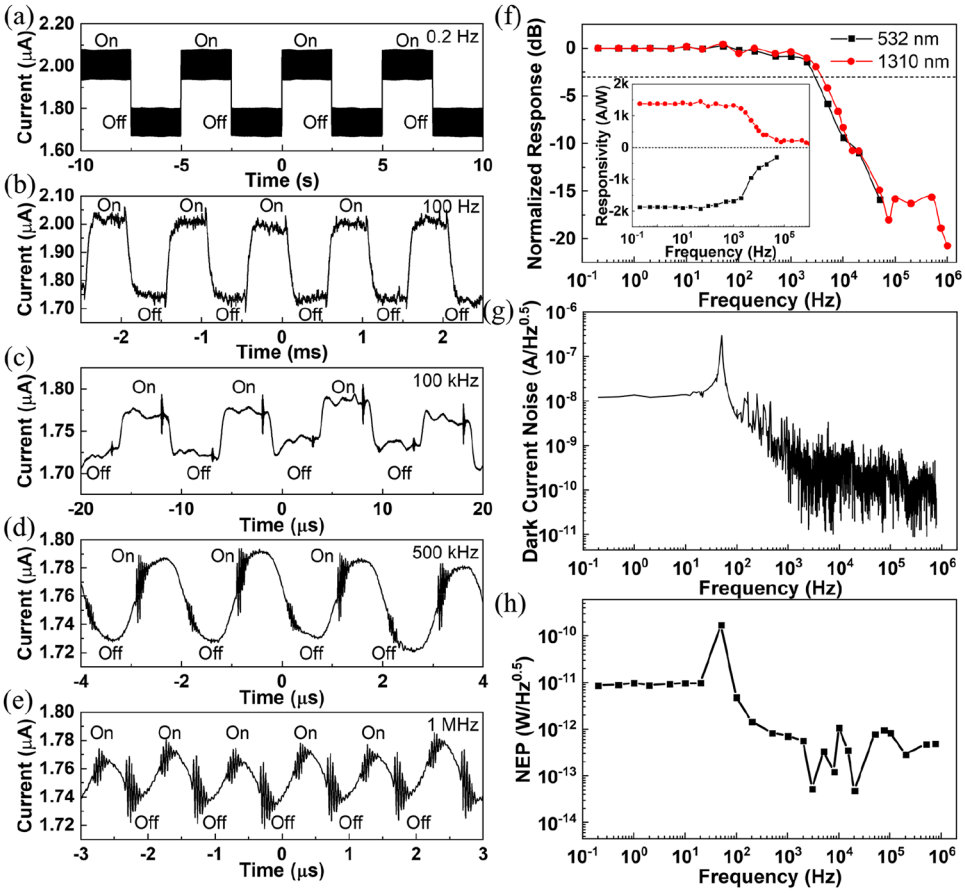

Figure 4. (a–e) The transient photoresponses of Ge/Si nanowire under 1310 nm light at the frequency of 0.2 Hz, 100 Hz, 100 kHz, 500 kHz, and 1 MHz, respectively. (f) The −3 dB bandwidth. It is 2.9 kHz under 532 nm light with a power density of 0.01 W/cm^2 and 3.9 kHz under 1310 nm light with a power density of 0.41 W/cm^2. **Inset:** The responsivity of the nanowire as a function of frequency. (g) The dark current noise. (h) The noise equivalent power (NEP) using 1310 nm light. The nanowire used here has a channel width of 450 nm and a length of 10 μm at a fixed bias voltage of 0.1 V.

344.6 ns, implying a substantial suppression of surface recombination velocity in the nanowires.[26−28]

Figure 4 summarizes the frequency response and noise characteristics of the Ge/Si nanowire photodetector. Representative time-domain photoresponse waveforms measured under periodic optical modulation at different frequencies are shown in Figure 4(a–e). At low modulation frequencies, the device exhibits a stable and reproducible photocurrent signal with a well-defined amplitude. As the modulation frequency increases, the output signal gradually decreases due to the finite carrier transport and recombination dynamics in the nanowire channel. The 3 dB bandwidth is 2.9 kHz under 532 nm light and 3.9 kHz under 1310 nm light as shown in Figure 4(f). The gain−bandwidth product (GBW) of the nanowire photodetector was evaluated by multiplying the low-frequency photoconductive gain with the 3 dB cutoff frequency, yielding 5×10^6 Hz. To evaluate the noise performance, the dark current noise was characterized by recording the dark current in real time and performing a fast Fourier transform (FFT). The resulting current noise spectral density is shown in Figure 4(g). At low frequencies, the noise spectrum is dominated by 1/f noise, which is commonly observed in photodetectors. At higher frequencies, the noise spectral density approaches a frequency-independent white noise floor, indicating that thermal and shot noise become the dominant contributions. Based on the measured current noise spectral density and the device responsivity, the frequency-dependent noise-equivalent power (NEP) is calculated using $\mathrm{NEP}(f) = i_n(f)/R_i(f)$, where $i_n(f)$ is the current noise and $R_i(f)$ is the responsivity.[29] As shown in Figure 4(h), the NEP decreases with frequency in the low-frequency region due to the suppression of 1/f noise and reaches a minimum value in the white-noise-limited region. The minimum NEP is determined to be 5.3×10^{-14} W/Hz$^{0.5}$, corresponding to a specific detectivity of 4.0×10^9 Jones. This is a typical value for devices with photogain.[30,31]

To decipher the physical origin behind this negative and positive photoresponse, we measured the photocurrent through different pairs of electrodes. Figure 5(a,b) show the photocurrent through Ge channel. Large negative photocurrent λ = 532 nm and small positive photocurrent λ = 1310 nm are observed. The photocurrent is larger at visible wavelengths because the absorption coefficient is much larger at short wavelengths. The negative photoresponses at λ = 532 nm must come from the $Si_{1-x}Ge_x$ buffer layer and the bottom Si layer, as the photoresponses become positive when Si does not absorb light at λ = 1310 nm. This can be seen clearly in the optical power distributions in the nanowires as shown in the inset of Figure 5(a,b). At λ = 532 nm, most of the light will inevitably be reflected by germanium. Nevertheless, the power distribution of the light inside the nanowire is mainly concentrated in Si. The strong absorption in Si forward biases the $Si_{1-x}Ge_x$-Si PN junction. This forward-biased junction

https://doi.org/10.1021/acsphotonics.5c02680
ACS Photonics XXXX, XXX, XXX−XXX

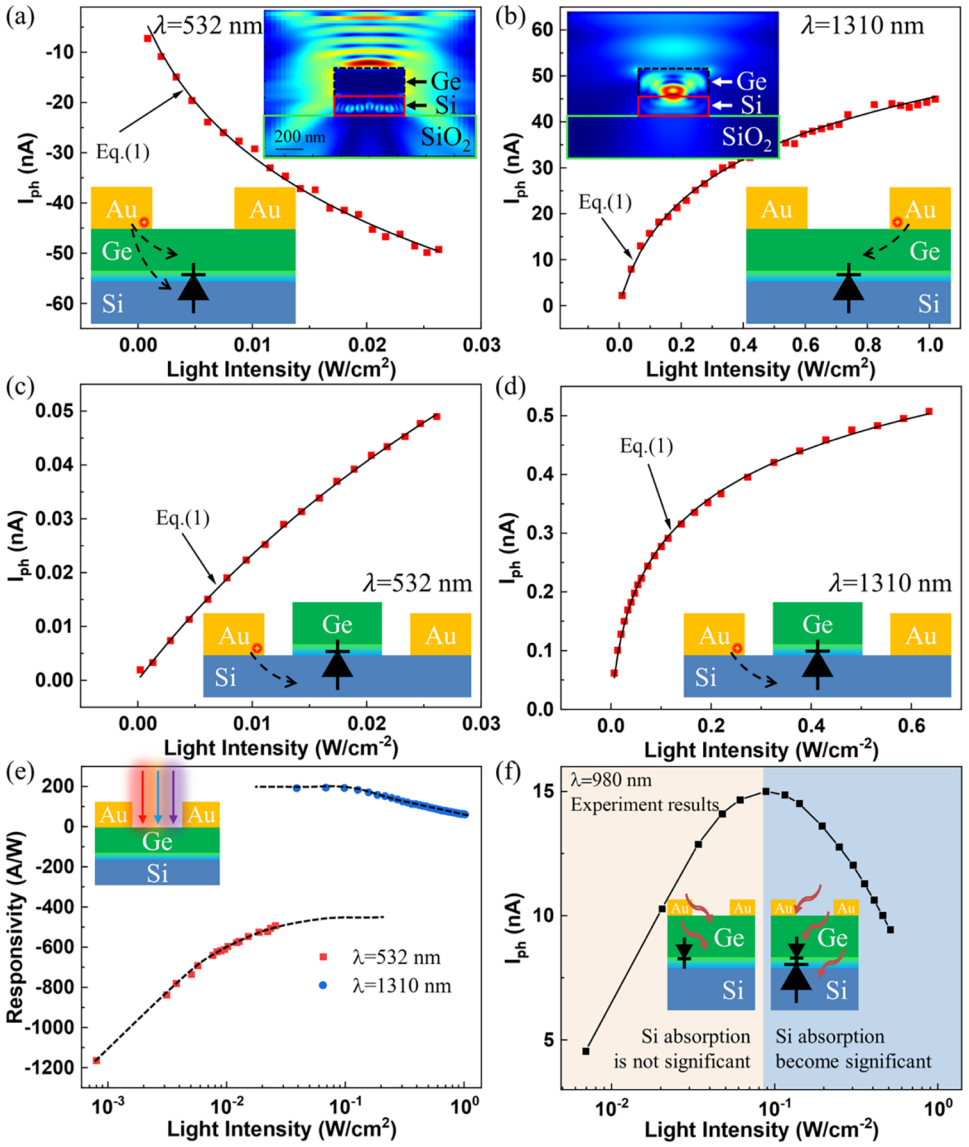

Figure 5. Photocurrent current as a function of light intensity with two contacts on germanium and using (a) 532 nm light that shows negative photoconductivity and (b) 1310 nm light that shows positive photoconductivity, respectively. **Inset**: The power distribution inside the Ge/Si nanowire under 532 and 1310 nm light in (a) and (b), respectively. Photocurrent current with two contacts on silicon using (c) 532 nm light and (d) 1310 nm light, respectively. Both cases show positive photoconductivity. Solid lines are fitted results using eq 1. (e) Negative responsivity of 532 nm light and positive responsivity of 1310 nm light. (f) Photocurrent through Ge channel as a function of light intensity using a 980 nm laser diode. The nanowire used here both are 450 nm wide and 10 μm long at a fixed bias voltage of 0.1 V.

Table 1. Extracted Parameters from Figure 5

	λ = 532 nm			λ = 1310 nm		
contact pads	I_{th} (nA)	P^s_{light} (mW/cm^2)	τ_0 (ns)	I_{th} (nA)	P^s_{light} (mW/cm^2)	τ_0 (ns)
Ge channel	−24.4 ± 1.1	4.0 ± 0.4	80.3 ± 7.6	16.1 ± 0.5	64.4 ± 4.6	5.1 ± 0.4
Si channel	0.07 ± 0.01	24.1 ± 1.7	13.1 ± 0.9	0.13 ± 0.01	12.6 ± 0.4	25.9 ± 0.8

pumps photoelectrons into the p-type Ge channel, creating a negative photoresponse in the Ge channel. In contrast, at λ = 1310 nm, the light is mainly concentrated in the upper Ge region. In this case, the Ge channel acts like a regular photoconductor, exhibiting positive photoresponses. Figure 5c,d show the photoresponses measured through the underlying Si layer. Transient data and corresponding photocurrent data at different voltages when silicon is used as the electrical contact can be found in SI Section X. These data prove that the positive photoresponse in this case is independent of the bias voltage of the device. Interestingly, both photoresponses at λ = 532 and 1310 nm are positive even though Si does not absorb light at wavelengths longer than 1.1 μm. This is attributed to the presence of the $Si_{1-x}Ge_x$ buffer layer. In the visible spectrum, light is strongly absorbed by Si. However, because the Si channel is partially depleted, its photoresponsivity is reduced in comparison with continuous-channel nanowire photoconductors. At λ = 1310 nm, although the optical mode is primarily localized in the Ge channel, part of the light will be absorbed by the $Si_{1-x}Ge_x$ buffer layer, which

https://doi.org/10.1021/acsphotonics.5c02680
ACS Photonics XXXX, XXX, XXX−XXX

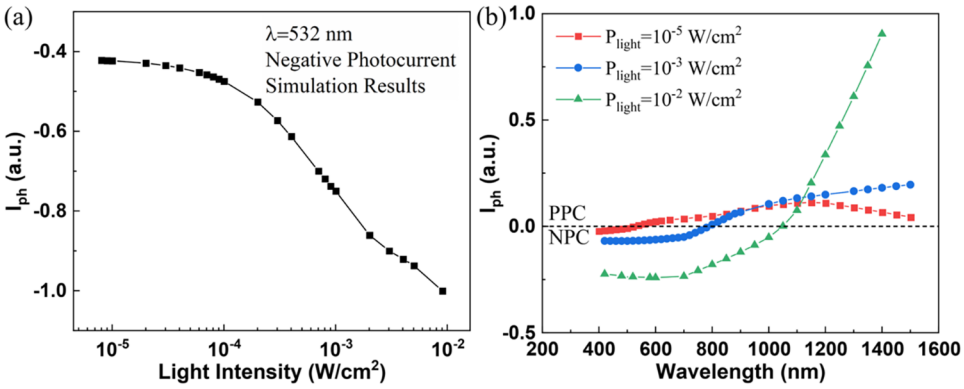

Figure 6. Simulation results of Ge/Si nanowire. (a) Photocurrent as a function of light intensity using 532 nm light. (b) Spectrum response of Ge/Si nanowires using different light intensities.

will modulate the Si channel, causing some weak photoresponses. The photoresponsivity of the Ge channel at these two wavelengths are plotted in Figure 5(e). Similar to the widely observed photoconductors, the photoresponsivity increases as the light intensity decreases, reaching 10^2 A/W for λ = 1310 nm and -10^3 A/W for λ = 532 nm.

The fitting curves are shown as the solid lines in Figure 5(a−d). The extracted parameters are summarized in Table 1. The threshold photocurrent I_{th} obtained from the negative photocurrent is negative. I_{th} will be larger for the Ge channel than the Si channel. For the Ge channel, we also observed that the critical light intensity P^{s}_{light} at λ = 1310 nm was greater by more than an order of magnitude than λ = 532 nm. However, for the Si channel, the P^{s}_{light} of these two wavelengths are comparable. The critical light intensity is inversely proportional to the minority carrier lifetime, according to our previous works.[21,24,25] The minority carrier lifetime of low-dimensional device is dominated by the surface recombination velocity.[26] For nanowires, the large surface-to-volume ratio will amplify the surface recombination velocity, significantly reducing the effective minority recombination lifetime from microseconds in bulk Si/Ge to nanoseconds in nanowires. This observation is consistent with many previous reports.[27]

To further validate the negative photoresponse mechanism above, the nanowire was illuminated with light at an intermediate wavelength of 980 nm, lying between 532 and 1310 nm. At weak light intensities, the light power reaching the $Si_{1-x}Ge_x$ and Si layers is negligible, similar to the case in Figure 5(b) at λ = 1310 nm. Under these conditions, the photoresponse is dominated by absorption in the Ge channel. As the light intensity increases, $Si_{1-x}Ge_x$ and Si layers start to absorb photons, activating the p−n junction and weakening the photoresponse in the Ge channel, as shown in Figure 5(f).

Finally, to verify the inference above, numerical simulations of Ge/Si heterojunction nanowires were performed using commercial Silvaco TCAD. Figure 6(a) shows the dependence of photocurrent on light intensity under 532 nm light, which is in good agreement with the experimental observations. Under 532 nm light, silicon provides additional electrons and attracts holes to reduce the conductivity of germanium nanowire. Figure 6(b) shows the spectral responses at different light intensities. The results indicate that the wavelength at which photocurrent becomes zero changes with the light intensity. Overall, this wavelength becomes longer as light power increases. This behavior arises because, at higher power levels, even long-wavelength light with relatively low absorption coefficients can generate sufficient carriers in silicon to modulate the conductive channel in germanium. Furthermore, within the wavelength range where silicon has extremely weak absorption, such as above 1310 nm, silicon no longer participates in the conductivity of the device by generating carriers. Consequently, at a fixed wavelength in this regime, the photocurrent increases monotonically with light intensity. In the intermediate wavelength range from approximately 800 to 1100 nm, the photocurrent exhibits a nonmonotonic dependence on light intensity at a fixed wavelength. In contrast, at wavelengths where silicon absorption is extremely weak, such as above 1310 nm, silicon no longer contributes to the device conductivity through photocarrier generation. Consequently, at a fixed wavelength in this regime, the photocurrent increases monotonically with light intensity. In the intermediate wavelength range from approximately 800 to 1100 nm, the photocurrent exhibits a nonmonotonic dependence on light intensity at a fixed wavelength, consistent with the experimental results shown in Figure 5(f).

CONCLUSION

In conclusion, we have successfully fabricated and characterized a Ge/Si heterojunction nanowire photodetector that exhibits a switchable and tunable photoresponse. The key finding of this work is the demonstration of a clear transition from Negative Photoconductivity (NPC) under visible illumination to Positive Photoconductivity (PPC) under near-infrared illumination. We have conclusively identified the physical mechanism behind this unique behavior: the competition between carrier generation within the Ge channel (causing PPC) and carrier injection from the Si layer into Ge via a light-induced forward bias of the heterojunction (causing NPC). The spectral absorption profile of the multilayer structure dictates which mechanism dominates.

This mechanistic understanding was validated by measuring photocurrent through different electrode configurations, analyzing the intensity-dependent response, and correlating the findings with optical mode simulations and TCAD device modeling. The excellent agreement between our experimental data and the established nanowire photoconductor model further solidifies our interpretation. The temperature-dependent measurement results further ruled out other mechanisms and confirmed our conclusion. The ability to control the photoresponse sign simply by varying the wavelength or intensity of light, coupled with the device's inherent compatibility with CMOS processes, opens new avenues for

https://doi.org/10.1021/acsphotonics.5c02680
ACS Photonics XXXX, XXX, XXX−XXX

innovative optoelectronic devices. Such devices could be employed in wavelength-selective switching, optical logic gates, and highly sensitive, multispectral sensing platforms. Future work will focus on optimizing the layer structure and doping profiles to enhance the responsivity and to explore the high-speed switching capabilities of this NPC-PPC transition.

■ ASSOCIATED CONTENT

Data Availability Statement

Data are available from the corresponding author upon reasonable request.

Supporting Information

The Supporting Information is available free of charge at https://pubs.acs.org/doi/10.1021/acsphotonics.5c02680.

Fabrication processes, the experimental testing and simulation methods, the SEM and EDS results, the $I-V$ curves of nanowires with different geometrical dimensions, the refractive index and extinction coefficient of each layer, the fitting results of bandgap, the Hall effect measurement results, the additional positive and negative photoconductivity experimental results, the fitting results of positive and negative photocurrents, the additional positive and negative responsivity, the photocurrent saturation phenomenon with bias voltage, the additional positive photocurrent and its fitting results when silicon is used as electrode contact (PDF)

■ AUTHOR INFORMATION

Corresponding Authors

Zhijuan Su − *Global Institute of Future Technology, Shanghai Jiao Tong University, Shanghai 200240, China*; Email: zhijuan.su@sjtu.edu.cn

Yaping Dan − *State Key Laboratory of Micro-Nano Engineering Science, Global College, Shanghai Jiao Tong University, Shanghai 200240, China*; orcid.org/0000-0002-2983-7213; Email: yaping.dan@sjtu.edu.cn

Authors

Huayou Liu − *State Key Laboratory of Micro-Nano Engineering Science, Global College, Shanghai Jiao Tong University, Shanghai 200240, China*; orcid.org/0000-0003-0942-9308

Jing Zhang − *State Key Laboratory of Micro-Nano Engineering Science, Global College, Shanghai Jiao Tong University, Shanghai 200240, China*

Jie-yin Zhang − *Institute of Physics, Chinese Academy of Sciences, Haidian, Beijing 100190, China; Songshan Lake Materials Laboratory, Dongguan, Guangzhou 523808, China*

Jiayuan Zhao − *State Key Laboratory of Micro-Nano Engineering Science, Global College, Shanghai Jiao Tong University, Shanghai 200240, China*

Constantinos Valagiannopoulos − *School of Electrical and Computer Engineering, National Technical University of Athens, Athens GR-15780, Greece*; orcid.org/0000-0003-1560-2576

Daniele Tosi − *School of Engineering and Digital Sciences, Nazarbayev University, Astana 010000, Kazakhstan*; orcid.org/0000-0002-6500-4964

Jian-jun Zhang − *Institute of Physics, Chinese Academy of Sciences, Haidian, Beijing 100190, China; Songshan Lake Materials Laboratory, Dongguan, Guangzhou 523808, China*

Complete contact information is available at: https://pubs.acs.org/10.1021/acsphotonics.5c02680

Funding

This work was financially supported by the National Natural Science Foundation of China (W2412118, 62574130) and the Oceanic Interdisciplinary Program of Shanghai Jiao Tong University (SL2022ZD107).

Notes

The authors declare no competing financial interest.

■ ACKNOWLEDGMENTS

The molecular beam epitaxy of germanium film on SOI was supported by the Institute of Physics Chinese Academy of Sciences. The patterning of nanowire was supported by the Advanced Electronic Materials and Devices (AEMD) of Shanghai Jiao Tong University.

■ REFERENCES

(1) Rogalski, A.; Martyniuk, P.; Kopytko, M. Challenges of small-pixel infrared detectors: a review. *Rep. Prog. Phys.* **2016**, *79* (4), No. 046501.

(2) Wang, J.; Ling, C.; Xue, X.; Ji, H.; Rong, C.; Xue, Q.; Zhou, P.; Wang, C.; Lu, H.; Liu, W. Self-Powered and Broadband Photodetectors Based on High-performance Mixed Dimensional Sb_2O_3/$PdTe_2$/Si Heterojunction for Multiplex Environmental Monitoring. *Small* **2024**, *20* (23), No. 2310107.

(3) Wu, Y.; Li, X.; Wei, Y.; Gu, Y.; Zeng, H. Perovskite photodetectors with both visible-infrared dual-mode response and super-narrowband characteristics towards photo-communication encryption application. *Nanoscale* **2018**, *10* (1), 359−365.

(4) Martyniuk, P.; Antoszewski, J.; Martyniuk, M.; Faraone, L.; Rogalski, A. New concepts in infrared photodetector designs. *Appl. Phys. Rev.* **2014**, *1* (4), No. 041102.

(5) Downs, C.; Vandervelde, T. E. Progress in Infrared Photodetectors Since 2000. *Sensors* **2013**, *13* (4), 5054−5098.

(6) Ren, A.; Yuan, L.; Xu, H.; Wu, J.; Wang, Z. Recent progress of III−V quantum dot infrared photodetectors on silicon. *J. Mater. Chem. C* **2019**, *7* (46), 14441−14453.

(7) LaPierre, R. R.; Robson, M.; Azizur-Rahman, K.; Kuyanov, P. A review of III−V nanowire infrared photodetectors and sensors. *J. Phys. D:Appl. Phys.* **2017**, *50* (12), No. 123001.

(8) Basu, P. K.; Das, N.; Mukhopadhyay, B.; Sen, G.; Das, M. K. Ge/Si photodetectors and group IV alloy based photodetector materials. *Opt. Quantum Electron.* **2009**, *41* (7), 567−581.

(9) Wang, J.; Lee, S. Ge-photodetectors for Si-based optoelectronic integration. *Sensors* **2011**, *11* (1), 696−718.

(10) Colace, L.; Masini, G.; Assanto, G. Ge-on-Si approaches to the detection of near-infrared light. *IEEE J. Quantum Electron.* **1999**, *35* (12), 1843−1852.

(11) Cui, B.; Xing, Y.; Han, J.; Lv, W.; Lv, W.; Lei, T.; Zhang, Y.; Ma, H.; Zeng, Z.; Zhang, B. Negative photoconductivity in low-dimensional materials. *Chin. Phys. B* **2021**, *30* (2), No. 028507.

(12) Chaves, A. S.; Chacham, H. Negative photoconductivity in semiconductor heterostructures. *Appl. Phys. Lett.* **1995**, *66* (6), 727−729.

(13) Tailor, N. K.; Aranda, C. A.; Saliba, M.; Satapathi, S. Negative photoconductivity: bizarre physics in semiconductors. *ACS Mater. Lett.* **2022**, *4* (11), 2298−2320.

(14) Yang, Y.; Peng, X.; Kim, H.-S.; Kim, T.; Jeon, S.; Kang, H. K.; Choi, W.; Song, J.; Doh, Y.-J.; Yu, D. Hot carrier trapping induced negative photoconductance in InAs nanowires toward novel non-volatile memory. *Nano Lett.* **2015**, *15* (9), 5875−5882.

(15) Lui, C.; Frenzel, A.; Pilon, D.; Lee, Y.-H.; Ling, X.; Akselrod, G.; Kong, J.; Gedik, N. Trion-induced negative photoconductivity in monolayer MoS_2. *Phys. Rev. Lett.* **2014**, *113* (16), No. 166801.
(16) Burdanova, M. G.; Tsapenko, A. P.; Satco, D. A.; Kashtiban, R.; Mosley, C. D.; Monti, M.; Staniforth, M.; Sloan, J.; Gladush, Y. G.; Nasibulin, A. G.; Lloyd-Hughes, J. Giant negative terahertz photoconductivity in controllably doped carbon nanotube networks. *ACS Photonics* **2019**, *6* (4), 1058−1066.
(17) Zhao, S.; Sun, J.; Yin, Y.; Guo, Y.; Liu, D.; Miao, C.; Feng, X.; Wang, Y.; Xu, M.; Yang, Z.-x. In situ growth of GeS nanowires with sulfur-rich shell for featured negative photoconductivity. *J. Phys. Chem. Lett.* **2021**, *12* (12), 3046−3052.
(18) Dan, Y.; Zhao, X.; Chen, K.; Mesli, A. A photoconductor intrinsically has no gain. *ACS Photonics* **2018**, *5* (10), 4111−4116.
(19) Fischetti, M. V.; Laux, S. E. Band structure, deformation potentials, and carrier mobility in strained Si, Ge, and SiGe alloys. *J. Appl. Phys.* **1996**, *80* (4), 2234−2252.
(20) Jacoboni, C.; Nava, F.; Canali, C.; Ottaviani, G. Electron drift velocity and diffusivity in germanium. *Phys. Rev. B* **1981**, *24* (2), No. 1014.
(21) Miao, J.; Song, B.; Li, Q.; Cai, L.; Zhang, S.; Hu, W.; Dong, L.; Wang, C. Photothermal Effect Induced Negative Photoconductivity and High Responsivity in Flexible Black Phosphorus Transistors. *ACS Nano* **2017**, *11* (6), 6048−6056.
(22) Zheng, K.; Luo, L.-B.; Zhang, T.-F.; Liu, Y.-H.; Yu, Y.-Q.; Lu, R.; Qiu, H.-L.; Li, Z.-J.; Andrew Huang, J. C. Optoelectronic characteristics of a near infrared light photodetector based on a topological insulator Sb_2Te_3 film. *J. Mater. Chem. C* **2015**, *3* (35), 9154−9160.
(23) Mahapatra, A.; Anilkumar, V.; Chavan, R. D.; Yadav, P.; Prochowicz, D. Understanding the Origin of Light Intensity and Temperature Dependence of Photodetection Properties in a $MAPbBr_3$ Single-Crystal-Based Photoconductor. *ACS Photonics* **2023**, *10* (5), 1424−1433.
(24) Wang, L.; Wang, J.; Liu, C.; Xu, H.; Li, A.; Wei, D.; Liu, Y.; Chen, G.; Chen, X.; Lu, W. Distinctive Performance of Terahertz Photodetection Driven by Charge-Density-Wave Order in CVD-Grown Tantalum Diselenide. *Adv. Funct. Mater.* **2019**, *29* (45), No. 1905057.
(25) He, J.; Chen, K.; Huang, C.; Wang, X.; He, Y.; Dan, Y. Explicit gain equations for single crystalline photoconductors. *ACS Nano* **2020**, *14* (3), 3405−3413.
(26) He, J.; Liu, H.; Huang, C.; Jia, Y.; Li, K.; Mesli, A.; Yang, R.; He, Y.; Dan, Y. Analytical transient responses and gain−bandwidth products of low-dimensional high-gain photodetectors. *ACS Nano* **2021**, *15* (12), 20242−20252.
(27) Dan, Y.; Seo, K.; Takei, K.; Meza, J. H.; Javey, A.; Crozier, K. B. Dramatic reduction of surface recombination by in situ surface passivation of silicon nanowires. *Nano Lett.* **2011**, *11* (6), 2527−2532.
(28) Liu, H.; Dan, Y. Explicit Photogain Theory for Nanowire Photoconductors Validated by TCAD Software Simulations. *IEEE Trans. Electron Devices* **2023**, *70* (7), 3630−3636.
(29) Pecunia, V.; Anthopoulos, T. D.; Armin, A.; Bouthinon, B.; Caironi, M.; Castellanos-Gomez, A.; Chen, Y.; Cho, K.; Clegg, C.; Fang, X.; et al. Guidelines for accurate evaluation of photodetectors based on emerging semiconductor technologies. *Nat. Photonics* **2025**, *19* (11), 1178−1188.
(30) Conley, B. R.; Margetis, J.; Du, W.; Tran, H.; Mosleh, A.; Ghetmiri, S. A.; Tolle, J.; Sun, G.; Soref, R.; Li, B.; et al. Si based GeSn photoconductors with a 1.63 A/W peak responsivity and a 2.4 μm long-wavelength cutoff. *Appl. Phys. Lett.* **2014**, *105* (22), No. 221117.
(31) Wang, F.; Zhang, T.; Xie, R.; Liu, A.; Dai, F.; Chen, Y.; Xu, T.; Wang, H.; Wang, Z.; Liao, L.; et al. Next-Generation Photodetectors beyond Van Der Waals Junctions. *Adv. Mater.* **2024**, *36* (3), No. 2301197.

https://doi.org/10.1021/acsphotonics.5c02680
ACS Photonics XXXX, XXX, XXX−XXX